Synthesis, Crystal and Electronic Structure, and Thermal Conductivity Investigation of the Hollandite-like CsxCr5Te8 Phases (0.73 < x < 1)

Hugo Bouteiller, Bruno Fontaine, Takao Mori, Franck Gascoin, Jean-François Halet, David Berthebaud

Synthesis, Crystal and Electronic Structure, and Thermal Conductivity Investigation of the Hollandite-like $Cs_xCr_5Te_8$ Phases ($0.73 < x < 1$)

Hugo Bouteiller,[1,2,3] Bruno Fontaine,[4,5] Takao Mori,[3,6] Franck Gascoin,[1] Jean-François Halet,[2,*] and David Berthebaud[2,7,*]

[1] Laboratoire CRISMAT, ENSICAEN, UNICAEN, CNRS, Normandie Univ. (UMR 6508), Caen, France

[2] CNRS–Saint-Gobain–NIMS, IRL 3629, Laboratory for Innovative Key Materials and Structures (LINK), National Institute for Materials Science (NIMS), Tsukuba 305-0044, Japan

[3] Research Center for Materials Nanoarchitectonics (MANA), National Institute for Materials Science (NIMS), 1-1 Namiki, 305-0044 Tsukuba, Japan

[4] Univ Rennes, CNRS, Ecole Nationale Supérieure de Chimie de Rennes (ENSCR), Institut des Sciences Chimiques de Rennes (ISCR), UMR 6226, F-35000 Rennes, France

[5] Saint-Cyr Coëtquidan Military Academy, CReC, F-56380 Guer, France

[6] Graduate School of Pure and Applied Sciences, University of Tsukuba, Tsukuba 305-8671, Japan

[7] Nantes Université, CNRS, Institut des Matériaux de Nantes Jean Rouxel, IMN, F-44000 Nantes, France

ABSTRACT:

This article discusses a comprehensive study on the synthesis, structural and thermal conductivity properties of cesium-inserted chromium tellurides of formula $Cs_xCr_5Te_8$. Single crystals of three different compositions (x = 0.73, 0.91, and 0.97) were successfully synthesized and suggested the existence of a solid solution in the range $0.73 < x < 1$. Through a detailed single crystal characterization, the complete structure of these compounds is determined, revealing a distinct *B*-type hollandite-like structural form derived from the hollandite structure, in contrast to the more commonly observed *A*-type pseudo-hollandite in AM_5X_8-type chalcogenides (A = cation, M = transition metal, X = chalcogen). Periodic density functional theory calculations predict the $Cs_{0.73}Cr_5Te_8$ composition as the most stable one with a metallic conductive behavior. The thermal conductivity of bulk $Cs_xCr_5Te_8$ samples is measured to be 1.4 $W.m^{-1}.K^{-1}$ at 300 K and increases with temperature up to 2 $W.m^{-1}.K^{-1}$ at 673 K.

INTRODUCTION

Transition metal chalcogenides (TMCs) have been extensively studied for their wide range of properties and potential applications, including superconductivity,[1] optoelectronics,[2,3] photocatalysis,[4] and energy storage.[5] One of the key factors contributing to their diverse properties is their complex structural diversity, which often manifests as low-dimensional arrangements.[6,7] These structures can be characterized by the presence of two-dimensional (2D) sheets or one-dimensional (1D) infinite channels, often featuring spacious voids as observed in compounds like $AgCrSe_2$ [8,9] or Nb_3Se_4.[10] Such structural features are particularly attractive in the field of thermoelectricity where a very low thermal conductivity is required.[11] Indeed, the lattice component (κ_l) of the thermal conductivity is primarily governed by phonon scattering which is generally large in highly complex structures.[12,13] Consequently, an efficient strategy to reach low thermal conductivity is to aim at synthesizing low-dimensional structures containing large scattering centers in order to reduce effectively the phonon mean free path.[14–18] This is the case for instance of the chromium chalcogenide compounds $Tl_xCr_5Se_8$[15] and $Ba_{0.5}Cr_5Se_8$,[16] which exhibit remarkably low thermal conductivities of 0.7 $W.m^{-1}.K^{-1}$ and 0.8 $W.m^{-1}.K^{-1}$ at 300 K, respectively. Motivated by these findings, we have conducted a complete study on related compounds possessing similar structural features, with the aim of exploring their potential in thermoelectric applications.

The two aforementioned compounds belong to the family of hollandite derivatives materials, characterized by the general formula AM_5X_8 (A = Li–Cs, Sr, Ba, Cd, In, Tl, Sn, and Pb; M = Sc, Ti, V, Cr; and X = S, Se, Te).[14–41] The structure of these compounds is somewhat related to that of the hollandite mineral oxide $BaMn_8O_{16}$. First described by Byström and Byström,[42] the hollandite structure consists of interconnected chains of MnO_6 octahedra, where the chains share corners,

forming a quasi-one-dimensional framework. This arrangement gives rise to two distinct channels along the same axis direction. Barium cations, sitting in the largest channels, counterbalance the charge of the anionic framework and stabilize the structure (**Figure 1**a).

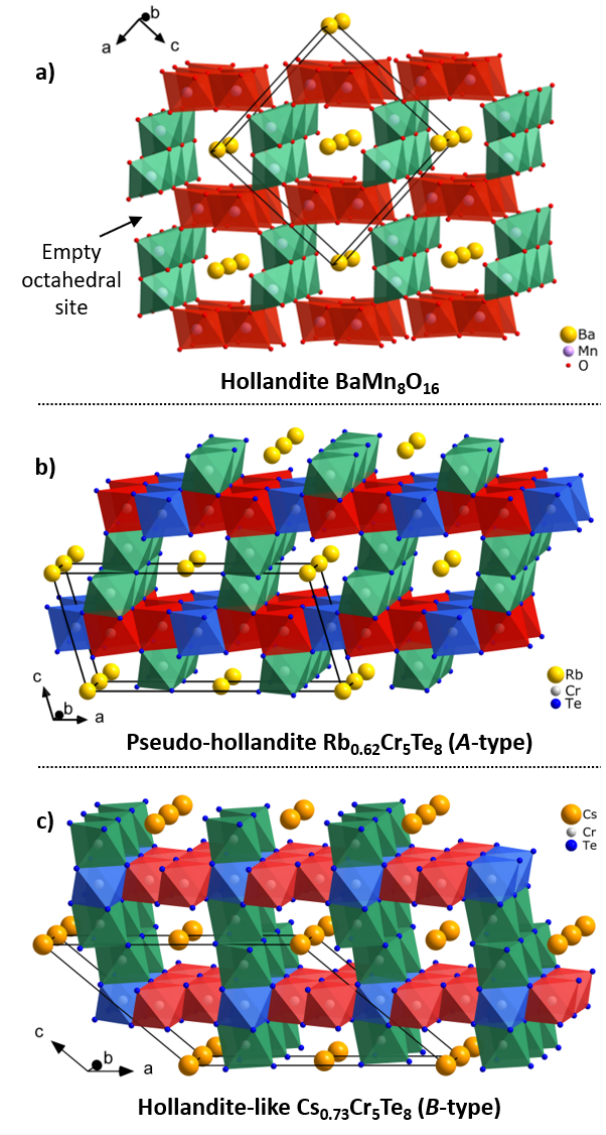

Figure 1. Structural representations of a) hollandite mineral,[43] b) pseudo-hollandite $Rb_{0.62}Cr_5Te_8$ (*A*-type, [35]) and c) hollandite-like $Cs_{0.73}Cr_5Te_8$ (*B*-type, this work). In the hollandite structure, the octahedral sites at the intersection of the double chains are unoccupied, resulting in the absence of a face-sharing octahedral arrangement. In hollandite derivatives (*A* and *B* types), where face-sharing octahedra are present, $CrTe_6$

octahedra corresponding to equivalent Cr1, Cr2 and Cr3 chromium atoms are depicted in blue, red and green, respectively. The same color scheme is used for all hollandite and hollandite derivatives structures to emphasize their related structural features. The size of the chalcogenide atoms is reduced for clarity.

Pseudo-hollandite compounds, such as $TlCr_5Se_8$,[20] derive from this parent hollandite mineral. Their structure involves the stacking of two dimensional CdI_2-like layers, where MX_6 octahedra share edges. These layers are interconnected by double chains of edge- and face-sharing MX_6 octahedra. The resulting framework forms large infinite channels along the monoclinic *b*-axis, with the cation A located at the center. Consequently, the small channels formed by the empty octahedral sites at the intersection of the double chains are absent in the pseudo-hollandite structure. These voids are filled with MX_6 octahedra, forming a continuous two-dimensional layer. This feature explains the stoichiometry difference between hollandite and pseudo-hollandite compounds. Furthermore, the filled octahedral sites involve face-sharing octahedra at the junction between the CdI_2-type layers and define the mode of connection between each layer in these hollandite derivatives (**Figure 1**b).

Boucher et al. demonstrated by investigating $Rb_{0.73}Cr_5Te_8$ the existence of another structural type referred to as "hollandite-like", which also originates from the parent hollandite.[35] This structure is still built up from 2D layers of $CrTe_6$ edge-sharing octahedra interconnected by pillaring double chains of face- and edge-sharing $CrTe_6$ octahedra, resulting in the same chemical formula as pseudo-hollandites. However, the way in which the two-dimensional layers interconnect differs. The "hollandite-like" structure can be described as a hollandite structure with a $CrTe_6$ octahedra occupying the octahedral voids present at the intersection of the double chains (**Figure 1**c). Yamazaki and Ueda[32] confirmed the existence of this second structural ‘hollandite-

like' arrangement and proposed the designations "*A*-type" for pseudo-hollandite compounds and "*B*-type" for the "hollandite-like" structures. This nomenclature is adopted in our study.

It is worth noting that among the extensive range of hollandite derivative compounds reported to date, only Rb_x- and Cs_x-inserted chromium tellurides ($x > 0.73$) adopt the 'hollandite-like' *B*-type structure, while all others crystallize in the 'pseudo-hollandite' *A*-type structure. Furthermore, deviations from stoichiometry are commonly observed in most of the hollandite derivatives, regardless of the *A* or *B* structure type.[15–17,27,28,34,35,37,39,44–47] In the case of chromium tellurides, the amount of A cations inside the channels influences the observed structural type and the determination of the tipping stoichiometry for the formation of one or the other structure type proves to be challenging. For instance, $Rb_{0.62}Cr_5Te_8$ crystallizes in the *A*-type structure whereas $Rb_{0.73}Cr_5Te_8$ adopts the *B*-type structure. Conversely, the non-stoichiometric chromium selenides $Rb_{0.75}Cr_5Se_8$ and $Cs_{0.76}Cr_5Se_8$ were reported to crystallize in the *A*-type structure.[39] This suggests that the *B* structural type is favored by (i) extended channels formed by large anions such as tellurium and (ii) large size cations such as Rb and Cs. Consistently, Yamazaki and Ueda[32] stated that the larger the amount of Rb, the more favored the *B*-type structure. However, no detailed structural determination was performed concerning the Cs-inserted chromium tellurides, nor the influence of the stoichiometric deviation on the structural features of these compounds. In this study, we report for the first time a complete crystal structure determination of a range of $Cs_xCr_5Te_8$ compounds ($x = 0.73$; 0.91; 0.97) synthesized as single crystals by two different routes. The impact of non-stoichiometry on the structural features is explored and compared through electronic structure calculations and crystal structure determination, enabling a discussion on the structural stability of specific compositions. Subsequently, the transport properties of these compounds are assessed and compared with those of other compounds.

EXPERIMENTAL SECTION

Synthesis and Preparation. Single crystals of $Cs_xCr_5Te_8$ with different compositions were grown using the self-flux method in fused silica tubes. The series of compounds was synthesized using two different routes. On the one hand, $Cs_{0.73}Cr_5Te_8$ and $Cs_{0.97}Cr_5Te_8$ single crystals were obtained by loading the $CsCr_5Te_8$ nominal composition from Cs_2CO_3 (powder, 99.9%), Cr (powder, 99.9%), and Te (shots, 99.999%) reagents under Ar atmosphere in a fused silica tube. After the tubes were flame-sealed under dynamic vacuum, temperature was raised to 500 °C over 8 hours, then to 800 °C over 8 hours and kept constant for 48 hours. Samples were then cooled to 200 °C over 8 days. On the other hand, $Cs_{0.91}Cr_5Te_8$ single crystals were grown from a different Cs precursor. $CsTe_4$ was first synthesized in a niobium tube by mixing appropriate amounts of Cs (metal, 99.8%) and Te (shots, 99.999%) within a glovebox. The niobium tube was then sealed under high purity argon within an arc furnace set up and placed inside a fused silica tube which was subsequently flame-sealed under dynamic vacuum. The sample was then heated over 10 hours at 300 °C for 96 hours, and cooled to room temperature over 10 hours. Mixture of $CsTe_4$, Cr (powder, 99.9%), and Te (shots, 99.999%) were loaded in a fused silica tube with the $CsCr_5Te_8$ nominal composition and sealed in a similar manner. The temperature was raised to 500 °C over 8 hours and kept constant for 8 hours. After this plateau, temperature was raised again over 8 hours at 800 °C and maintained for 24 hours, before cooling down the sample to 200 °C over a period of 96 hours. Black metallic-like needles were obtained by both synthesis routes.

Bulk samples of $Cs_xCr_5Te_8$ were prepared by mixing Cs_2CO_3 (powder, 99.9%), Cr (powder, 99.9%), and Te (shots, 99.999%) in a glovebox with appropriate amounts to obtain the $Cs_{0.73}Cr_5Te_8$ stoichiometry. The mixture was introduced in a 65-cm^3 stainless steel jar with two balls (Ø 12.6

mm) and underwent a run of 10 hours under argon atmosphere in a vibratory ball milling equipment (SPEX). The obtained powder was subsequently sintered by Spark Plasma Sintering (SPS) at 700 °C and the densified pellet was annealed at 700 °C during 24 hours. The relative density of the densified bulk material was 96 %. Powder X-ray diffraction pattern refinement was carried out by the Le Bail method using the Fullprof Suite,[48] yielding R_p = 11.3 %, R_{wp} = 15.3 % and χ^2 = 1.81 agreement factors (14 parameters). Thermal conductivity measurements were performed under N_2 atmosphere using a Netzsch 467 HyperFlash Laser-Flash Apparatus (LFA) on 10-mm diameter and 1-mm thick sample coated with graphite. Heat capacity was estimated according to the Dulong-Petit law and density was measured by the Archimede method in high purity ethanol.

Single Crystal Characterization. Single crystals of appropriate size for X-ray investigation were picked up in air and isolated in silicon oil, before being loaded on the goniometric head of a four-circle Rigaku XtaLAB Synergy-S diffractometer equipped with a molybdenum radiation source (λ_{Mo} = 0.71073 Å). The CrysAlis-Pro software[49] was used to analyze the collected data. Three-dimensional peak hunting was made before the subsequent data reduction corrected for absorption. Only reflections with $I > 3\sigma(I)$ were used for the charge-flipping structure resolution from SUPERFLIP[50] alongside the following refinement performed with Jana2006 software.[51] All parameters were refined with an instability factor of 0.025. Atomic displacement parameters (ADP) were refined anisotropically.

Electronic Structure Calculations. Periodic spin-polarized density functional theory (DFT) calculations were carried out in order to gain insight into the structural and electronic properties of the $Cs_xCr_5Te_8$ phases. Geometry optimizations were first performed on the stoichiometric $CsCr_5Te_8$ and non-stoichiometric $Cs_{0.75}Cr_5Te_8$ compounds using the Vienna *ab initio* Simulation

(*VASP*) code,[52–54] with the Perdew–Burke–Ernzerhof (PBE) functional.[55] VASP-relaxed structures were then used to compute the electronic density of states (DOS) with the *WIEN2k* code using the full-potential linearized augmented plane wave (FLAPW) approach,[56] employing the modified Becke-Johnson (mBJ) exchange-correlation potential.[57]

RESULTS AND DISCUSSION

$Cs_xCr_5Te_8$ (x = 0.73, 0.91, 0.97) Structures. All $Cs_xCr_5Te_8$ compounds (x = 0.73, 0.91, 0.97) were found to adopt the hollandite-like *B*-type structure with the space group *C*2/*m* (**Figure 1**c). Initially, the structures were solved by structure visualization, assuming a stoichiometric composition of $CsCr_5Te_8$ based on the nominal composition. However, akin to the structure resolution of $Rb_{0.73}Cr_5Te_8$ conducted by Gareh et al.,[34] Fourier difference maps revealed large electronic residues on the Cs 2*a* site, accompanied by high atomic displacement parameters. These observations suggested a possible deviation from stoichiometry, similar to $Rb_xCr_5Te_8$ compounds (x = 0.5, 0.62, and 0.73).[32,34,35] Subsequent refinement of the Cs site occupancy significantly reduced the electronic residues and improved the reliability factors for all crystals. Detailed crystallographic data collected for $Cs_{0.73}Cr_5Te_8$, $Cs_{0.91}Cr_5Te_8$ and $Cs_{0.97}Cr_5Te_8$ are given in **Table 1**. Pertinent interatomic distances of the investigated compounds are displayed and compared to those of $Rb_{0.73}Cr_5Te_8$ (*B*-type structure) in **Table 2**. The refined coordinates and atomic displacement parameters (ADPs) of the three compounds, along with their estimated standard deviation (esd), are available in the Supporting Information (**Tables 3, 4** and **5**, respectively).

Table 1. Crystallographic Data of $Cs_xCr_5Te_8$ Compounds (x = 0.73, 0.91, and 0.97)

Formula	$Cs_{0.73(1)}Cr_5Te_8$	$Cs_{0.91(1)}Cr_5Te_8$	$Cs_{0.97(1)}Cr_5Te_8$
Structural type	*B*	*B*	*B*

Molar mass (g.mol^{-1})	1378.1	1401.6	1409.6
Crystal system	Monoclinic	Monoclinic	Monoclinic
Space group	*C*2/*m* (12)	*C*2/*m* (12)	*C*2/*m* (12)
a (Å)	20.4192(7)	20.3889(11)	20.3573(6)
b (Å)	3.9248(1)	3.9574(2)	3.9634(1)
c (Å)	14.4962(4)	14.4496(8)	14.4331(12)
β (°)	139.872(4)	139.725(9)	139.730(7)
V (Å^3)	748.73(8)	753.70(16)	752.74(12)
Z	2	2	2
Calculated density (g.cm^{-3})	6.1125	6.1759	6.219
Data reduction			
No. of independent reflections	2218	1169	2736
No. of independent reflections with $I > 3\sigma(I)$	2026	957	2545
R_{int}	0.0354	0.0365	0.0382
Transmission factors	0.301 - 1	0.243 - 1	0.368 - 0.963
Refinement			
R_F (obs/all)	0.0184/0.0205	0.0259/0.0327	0.0233/0.0249
R_{WP} (obs/all)	0.0409/0.0422	0.0469/0.0492	0.0508/0.0522
Goodness of fit	1.30	1.34	1.70
No. of refined parameters	47	47	47
$\Delta\rho_{min}/\Delta\rho_{max}$ (e$^-$.Å^{-3})	-1.09/0.90	-1.49/1.34	-2.22/2.40

Table 2. Interatomic Distances of $Cs_xCr_5Te_8$ (x = 0.73, 0.91 and 0.97) and comparison with isostructural $Rb_{0.73}Cr_5Te_8$.[34]

	$Rb_{0.73}Cr_5Te_8$ [34]		**$Cs_{0.73}Cr_5Te_8$**		**$Cs_{0.91}Cr_5Te_8$**		**$Cs_{0.97}Cr_5Te_8$**	
$CrTe_2$ layer (ab plane)	Cr1–Te1	2.724(1) x 2	Cr1–Te1	2.7349(2) x 2	Cr1–Te1	2.7260(7) x 2	Cr1–Te1	2.7272(4) x 2
	Cr1–Te2	2.766(1) x 4	Cr1–Te2	2.7683(1) x 4	Cr1–Te2	2.7829(6) x 4	Cr1–Te2	2.7801(3) x 4
	Cr2–Te1	2.726(2) x 2	Cr2–Te1	2.7289(1) x 2	Cr2–Te1	2.733(2) x 2	Cr2–Te1	2.7306(5) x 2
	Cr2–Te2	2.752(2)	Cr2–Te2	2.7568(2)	Cr2–Te2	2.759(2)	Cr2–Te2	2.7572(7)
	Cr2–Te3	2.709(2) x 3	Cr2–Te3	2.7070(1) x 2	Cr2–Te3	2.709(2) x 2	Cr2–Te3	2.7093(5) x 2
			Cr2–Te3	2.7094(2)	Cr2–Te3	2.710(2)	Cr2–Te3	2.7088(6)
Bridging Cr–Te octahedra	Cr3–Te1	2.730(3)	Cr3–Te1	2.7474(1)	Cr3–Te1	2.746(2)	Cr3–Te1	2.7456(9)
	Cr3–Te2	2.775(1) x 2	Cr3–Te2	2.7777(1) x 2	Cr3–Te2	2.7853(7) x 2	Cr3–Te2	2.7795(4) x 2
	Cr3–Te4	2.695(3)	Cr3–Te4	2.7017(1)	Cr3–Te4	2.699 (2)	Cr3–Te4	2.702 (1)
	Cr3–Te4	2.715(2) x 2	Cr3–Te4	2.7133(1) x 2	Cr3–Te4	2.7198(7) x 2	Cr3–Te4	2.7198(3) x 2

A–Te	Rb–Te1	3.976(2) x 2	Cs–Te1	3.9752(4) x 2	Cs–Te1	3.9980(9) x 2	Cs–Te1	3.9865(6) x 2
	Rb–Te3	3.741(1) x 4	Cs–Te3	3.8313(2) x 4	Cs–Te3	3.8385(6) x 4	Cs–Te3	3.8384(4) x 4
	Rb–Te4	3.955(2) x 4	Cs–Te4	3.9888(1) x 4	Cs–Te4	3.9965(7) x 4	Cs–Te4	3.9935(3) x 4
Principal short Te–Te	Te1–Te2	3.781(1) x 2	Te1–Te2	3.8073(3) x 2	Te1–Te2	3.8116(7) x 2	Te1–Te2	3.8131(5) x 2
	Te1–Te3	3.747(2)	Te1–Te3	3.7610(1)	Te1–Te3	3.734(2)	Te1–Te3	3.7260(6)
Principal short Cr–Cr	Cr1–Cr3	3.069(2) x 2	Cr1–Cr3	3.1037(3) x 2	Cr1–Cr3	3.101 (2) x 2	Cr1–Cr3	3.0925(6) x 2
Principal short A–A	Rb–Rb	3.931(2) x 2	Cs–Cs	3.9248(1) x 2	Cs–Cs	3.9574(2) x 2	Cs–Cs	3.9634(1) x 2

The *B*-type structural feature found for this range of composition $Cs_xCr_5Te_8$ ($x = 0.73, 0.91, 0.97$) is consistent with the results of Yamazaki and Ueda[32] which state from powder X-ray diffraction analysis a *B*-type structure for Cs-inserted chromium telluride hollandite derivatives. The cells parameters of all compounds, except β, show a linear-like evolution with the increase of the *b* axis and a decrease of the *a* and *c* axes upon an increasing amount of Cs (**Figure 2**). This supports the existence of a solid solution ranging from the $Cs_{0.73}Cr_5Te_8$ composition – identical to that observed for the *B*-type $Rb_{0.73}Cr_5Te_8$ – to the almost completely filled $Cs_{0.97}Cr_5Te_8$ composition. The decrease of *a* and *c* cell parameters with the Cs amount is caused by a slight distortion of the $CrTe_6$ octahedra in the vicinity of the Cs inserted cations, contracting the cell along these axis directions. This is illustrated by the increased distances between Cs and Te atoms as well as Te-Te distances in the channels (Te3 and Te4) (**Table 2**). On the other hand, the increase of *b* stems from the increase of the Cs-Cs distances upon Cs insertion inside the channels and gives rise to an increased cell volume overall. Between compositions $x = 0.73$ and $x = 0.91$, the cell volume experiences a 0.66% increase. While the cell volumes of the highly Cs-filled compositions ($x = 0.91$ and $x = 0.97$) are closely similar (753.70(16) and 752.74(12) $Å^3$, respectively), the slight decrease observed

with increasing Cs content can be attributed to a further contraction of the unit cell along the *a* and *c* axes.

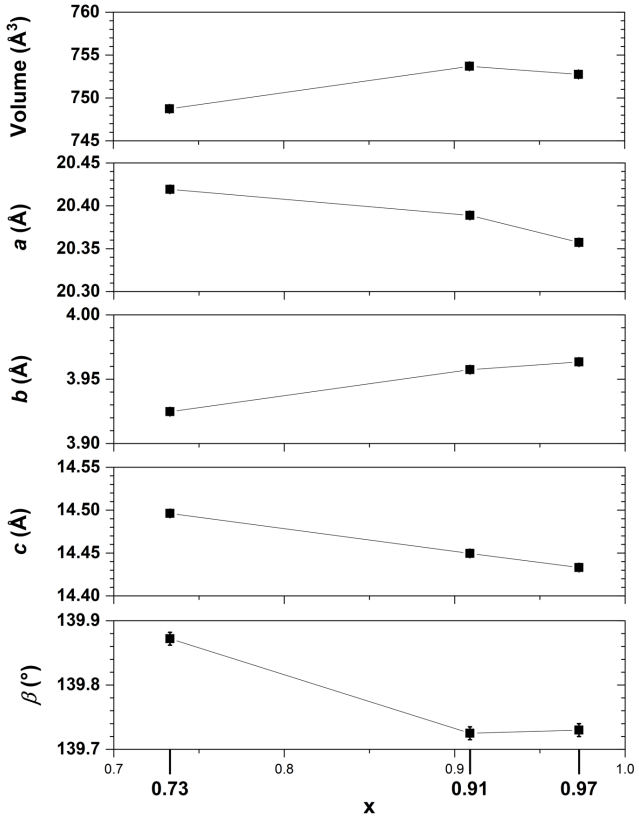

Figure 2. Evolution of cell parameters of the series of compounds $Cs_xCr_5Te_8$ (x = 0.73, 0.91, and 0.97) obtained from single-crystal X-ray diffraction measurements.

The atomic displacement parameters (ADPs) of the investigated compounds show notable characteristics. Indeed, the anisotropic ADP U_{22} along the *b* axis is significantly larger in $Cs_{0.73}Cr_5Te_8$ compared to the higher Cs-filled chromium tellurides (0.0853(5), 0.0347(5), 0.0246(2) Å^2 for x = 0.73, 0.91, and 0.97, respectively). This observation clearly indicates a high degree of disorder in the Cs distribution within the channels of the non-stoichiometric $Cs_{0.73}Cr_5Te_8$ compound. In contrast, the channel axis-oriented Cs ADP U_{22} rapidly decreases for $Cs_{0.91}Cr_5Te_8$ and becomes similar to other directional ADPs in $Cs_{0.97}Cr_5Te_8$, suggesting an isotropic ADP and reduced cationic disorder for the nearly fully occupied $Cs_xCr_5Te_8$ compound. These findings are

consistent with the highly anisotropic ADP observed for the inserted cations in other non-stoichiometric hollandite derivatives,[28,39,44] including the *B*-type $Rb_{0.73}Cr_5Te_8$.[34]

Stability of the *B* Structural Type. A noteworthy feature of the *B*-type structure, adopted by all investigated $Cs_xCr_5Te_8$ compositions, is the interaction between Cr atoms from the octahedra situated at the intersection between the layers and the pillaring double chain of octahedra (**Figure 3**). As previously mentioned, the distinction between the *A*- and *B*-types is the configuration of the face-sharing bridging double chain of octahedra between the $CrTe_2$ sheets positioned in the *ab* plane. In the *A*-type structure exemplified by $Rb_{0.62}Cr_5Te_8$, the junction consists of two distinct face-sharing octahedra (depicted in red in **Figure 3**) originating from the $CrTe_2$ layer, resulting in two Cr2–Cr3 pairs of Cr–Cr interactions. Conversely, in the *B*-type structure, only one octahedron (represented in blue in **Figure 3**) is involved in the face-sharing octahedra junction with the upper and lower pillaring double chains. As a consequence, a linear three-atom chain Cr3–Cr1–Cr3 is formed in this structure type, with shorter Cr–Cr distances compared to the *A*-type structure. For instance, Cr–Cr distances in *A*-type $Rb_{0.62}Cr_5Te_8$ are somewhat longer than in *B*-type $Rb_{0.73}Cr_5Te_8$: 3.161(2) Å and 3.069(2) Å, respectively. As the preparative conditions were invoked to synthesize either *A*- or *B*-type Rb-inserted $Rb_xCr_5Te_8$,[34] no occurrence of any *A*-type $Cs_xCr_5Te_8$ compound was found in our work, regardless of the synthesis routes.

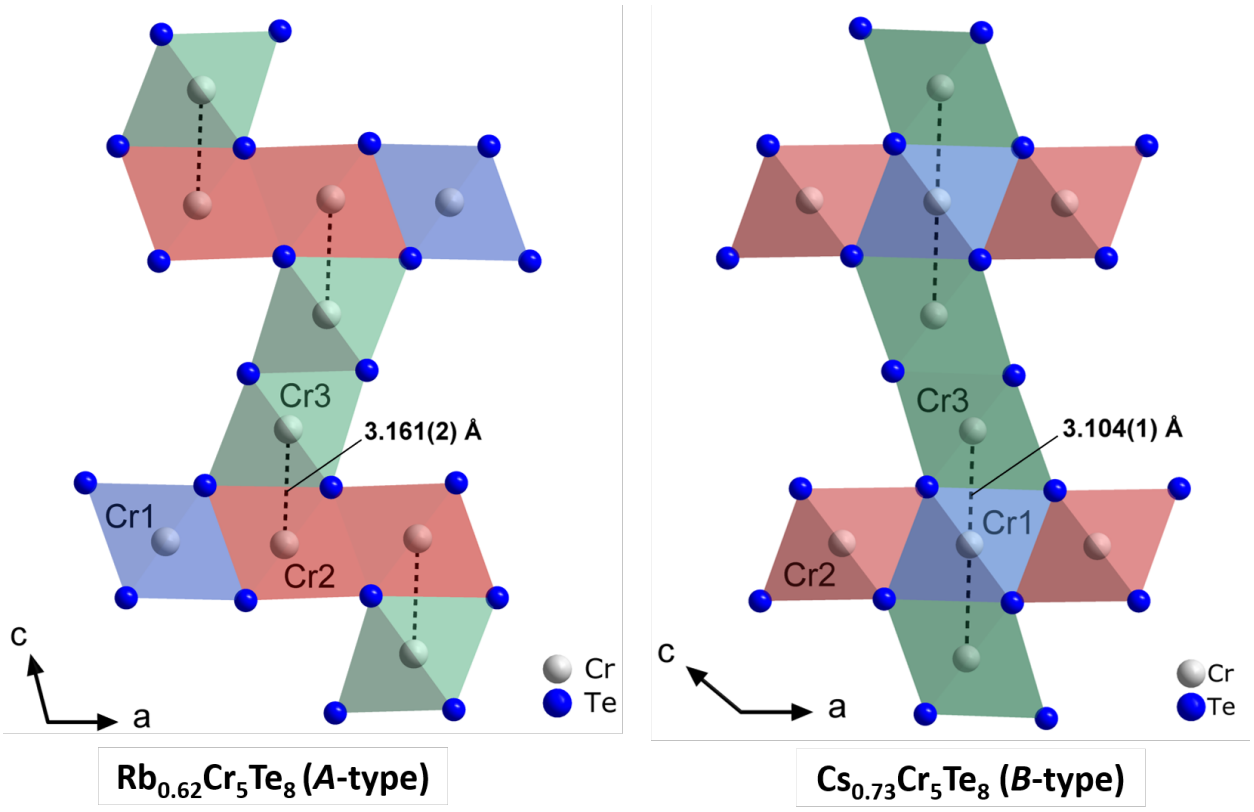

Figure 3. Description of the Cr–Cr interactions within the frameworks of $Rb_{0.62}Cr_5Te_8$ (*A*-type)[35] and $Cs_{0.73}Cr_5Te_8$ (*B*-type) structures. While the chromium atoms are interacting two by two in the *A*-type structure, those in the *B*-type undergo a three-by-three interaction with a shorter distance, resulting in an increased interaction in the latter.

Following the discussion of Boucher, Gareh and co-workers,[34,35] the weakly antibonding nature of the Cr–Cr interactions must explain the slight off-centering of the chromium atoms within their respective octahedra, as they somewhat repel each other. In the case of the *A*-type structure, the octahedra junction arrangement does not impose significant geometric restrictions on the chromium atoms, allowing them to have more freedom to repulse each other. However, this is not the case in the *B*-type structure, where the octahedron formed by Cr1 shares two faces with upper and lower pillaring octahedra, thereby restricting the freedom of Cr1 despite the antibonding nature

of its interaction with both the upper and lower Cr3 atoms. This crucial observation helps to elucidate why the *B*-type hollandite-like structure is not as commonly stabilized compared to the much more frequently encountered *A*-type pseudo-hollandites.

In the case of $Cs_xCr_5Te_8$ compounds reported in this work, the Cr–Cr distances are all longer than in $Rb_{0.73}Cr_5Te_8$. In particular, the Cr–Cr distance reaches 3.1037(3) Å in $Cs_{0.73}Cr_5Te_8$ to be compared to the somewhat shorter one (3.069(2) Å) in $Rb_{0.73}Cr_5Te_8$. It appears that this Cr–Cr distance decreases with increasing Cs content, with values of 3.101(2) Å and 3.0925(6) Å for $Cs_{0.91}Cr_5Te_8$ and $Cs_{0.97}Cr_5Te_8$, respectively. As the Cr–Cr interaction is overall weakly antibonding, the longer the Cr–Cr distance, the more stable the compound is expected to be. Hence, $Cs_{0.73}Cr_5Te_8$ should be more stable than higher Cs-filled chromium tellurides.

Periodic density functional theory (DFT) calculations were carried out on stoichiometric $CsCr_5Te_8$ and non- stoichiometric $Cs_{0.75}Cr_5Te_8$ compounds in order to elucidate their electronic and conducting properties. The computed total and Cs and Cr atom-projected spin-polarized electronic DOS are sketched in **Figure 4**. As discussed before for the $Rb_xCr_5Te_8$ phases,[35] spin-up and spin-down total and atom projected DOS strongly differ, suggesting magnetic properties which, unfortunately, have never been confirmed experimentally up to now. Interestingly, a favorable semiconducting behavior is computed for the stoichiometric $CsCr_5Te_8$ ($Cs^+[Cr_5Te_8]^-$) composition – this is almost reached for $Cs_xCr_5Te_8$ with $x = 0.97$ – with a strong participation of the Cr atoms and hardly any participation of the Cs cations. However, Boucher et al. have shown that for the $Rb_xCr_5Te_8$ phases,[35] Rb vacancies were expected to lower the Fermi level and to depopulate Cr–Cr non-bonding and antibonding states, favoring the structural stability of non-stoichiometric $Rb_xCr_5Te_8$ phases. The same situation occurs here for the non-stoichiometric $Cs_xCr_5Te_8$ compounds, i.e., partial depopulation of antibonding Cr–Cr states which enable to

somewhat stabilize the structure. As a consequence, the compounds are expected to show metallic properties with the Fermi level positioned in a substantial peak of DOS. It is interesting to mention that the interactions between chromium atoms appear to be crucial for the stabilization of *B*-type hollandite-like, as neither the stoichiometric $RbSc_5Te_8$,[41] $CsSc_5Te_8$[58] nor $CsTi_5Te_8$[40] compounds have been reported to crystallize in this structural form.

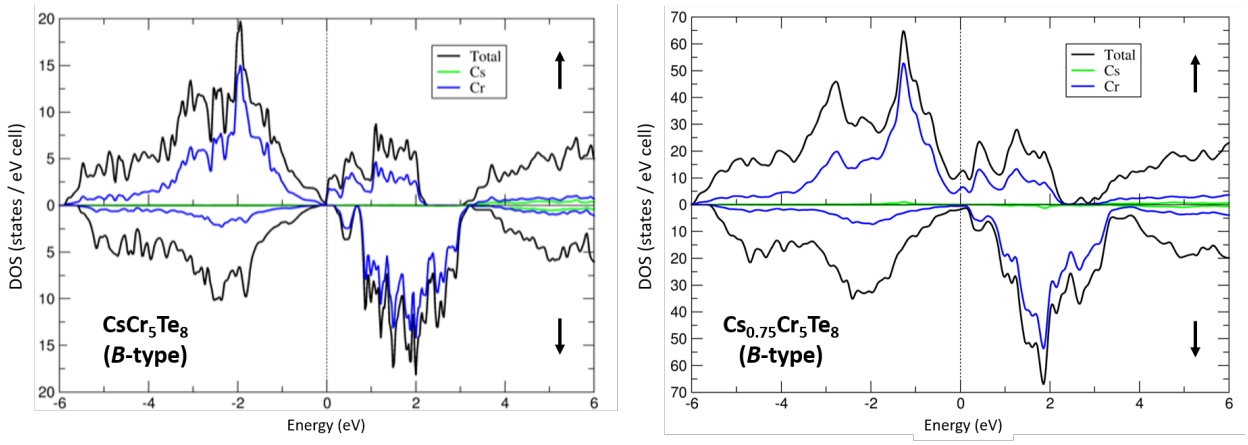

Figure 4. Spin-polarized total and atom-projected density of states of $CsCr_5Te_8$ (left) and $Cs_{0.75}Cr_5Te_8$ (right).

Bulk $Cs_xCr_5Te_8$ Preparation. In this study, efforts were made to synthesize high purity bulk materials with $Cs_{0.73}Cr_5Te_8$ and $CsCr_5Te_8$ compositions. Similar to the challenges encountered in the synthesis of $Rb_xCr_5Te_8$,[34] difficulties were faced in obtaining high purity samples. Nonetheless, a specimen of satisfactory purity was successfully synthesized, densified, and characterized by powder X-ray diffraction (**Figure 5**). The refined cell parameters of the predominant $Cs_xCr_5Te_8$ were determined to be a = 20.361(1) Å, b = 3.969(1) Å, c = 14.433(1) Å, β = 139.72(1) °, which closely align with the highly Cs-filled $Cs_xCr_5Te_8$ compound as determined by single-crystal structure analysis. As previously pointed out by Boucher et al. in their study on $Rb_xCr_5Te_8$,[35] the preparative conditions might have a significant importance in obtaining either non-stoichiometric (x < 1) or completely filled (x = 1) $Cs_xCr_5Te_8$ compounds. Our various synthesis routes suggest

that the optimal preparative conditions for $Cs_{0.73}Cr_5Te_8$ and $CsCr_5Te_8$ are highly similar, rendering difficult the control of the stoichiometry. Low-intensity reflections could be attributed to an unfilled Cr_5Te_8 impurity (space group $P\bar{3}m$). However, since Cr_5Te_8 exhibits metallic behavior,[59] as expected for $Cs_xCr_5Te_8$ as well, the presence of this impurity in the bulk is not believed to have a significant impact on the transport properties. It should be noted that the densified specimen showed sensitivity to oxidation and humidity, resulting in its degradation after a few days under ambient conditions. Nevertheless, thermal conductivity measurements were successfully performed on the sample before degradation occurred.

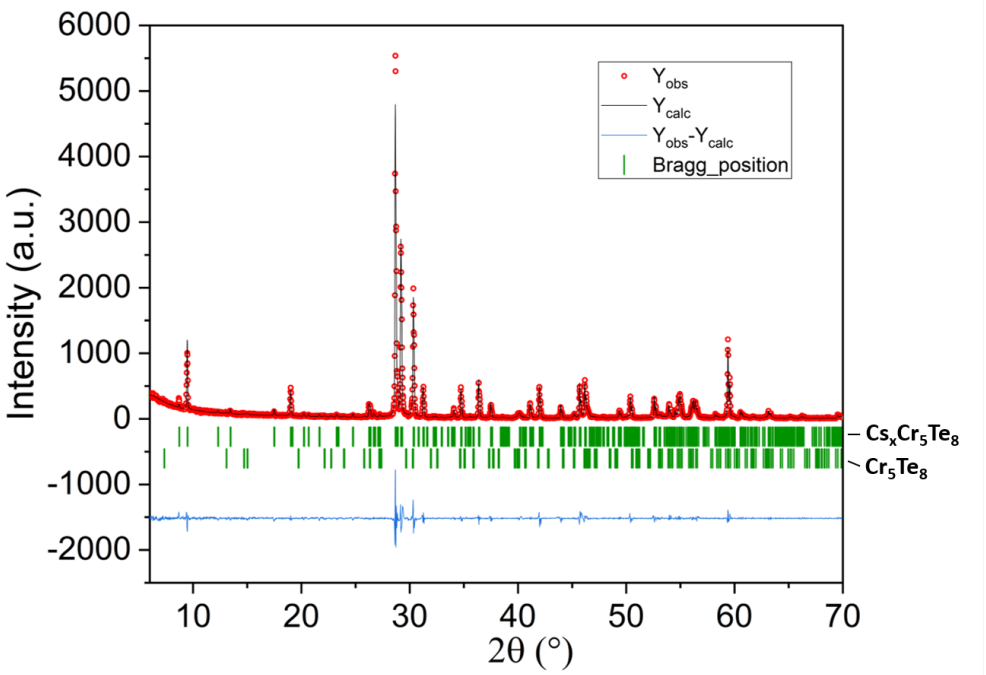

Figure 5. Le Bail refinement of the X-ray diffraction pattern of a densified and annealed $Cs_xCr_5Te_8$ sample. Low intensity additional reflections were attributed to a Cr_5Te_8 (space group $P\bar{3}m$) phase.

Thermal Conductivity Measurements. The temperature-dependent evolution of the thermal conductivity of the $Cs_xCr_5Te_8$ specimen is presented **Figure 6.** As depicted, the thermal conductivity increases from 1.4 $W.m^{-1}.K^{-1}$ at room temperature to approximately 2 $W.m^{-1}.K^{-1}$ at 673 K. In comparison with hollandite selenide derivatives, these values fall within an intermediate range. Specifically, they are lower than those measured for TlV_5Se_8, which shows a similar behavior but with values ranging from 2.5 to 3.3 $W.m^{-1}.K^{-1}$ in the same temperature range. Conversely, $Cs_xCr_5Te_8$ values are substantially higher than that of other *A*-type pseudo-hollandite $A_xM_5Se_8$ compounds (A = Ba, Tl, M = Cr, In), exhibiting thermal conductivities below 1 $W.m^{-1}.K^{-1}$. The difference is attributed to a higher electronic thermal conductivity due to the metallic character in the compounds TlV_5Se_8[18] and $Cs_xCr_5Te_8$.

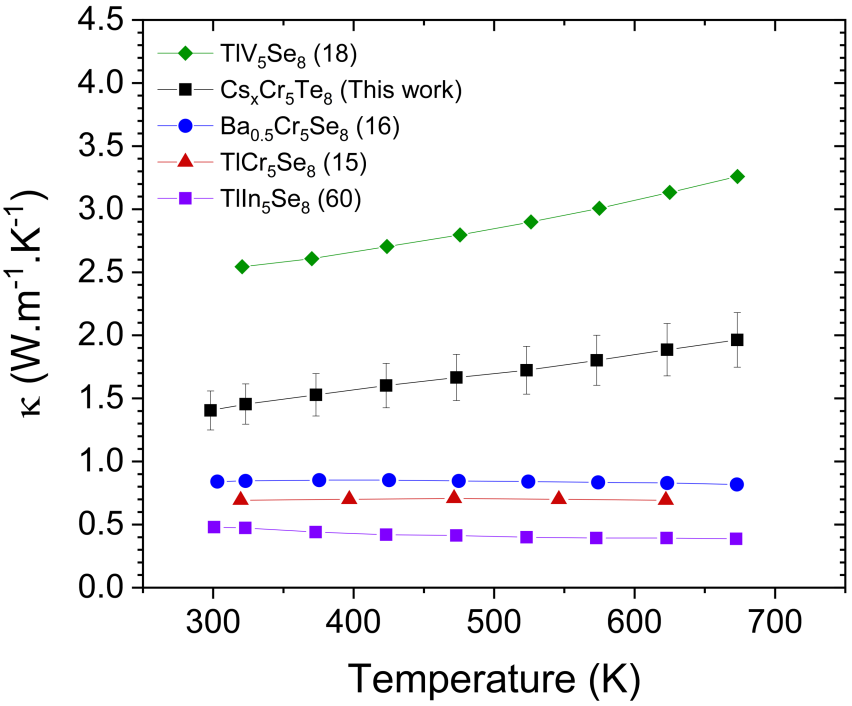

Figure 6. Thermal conductivity of *B*-type $Cs_xCr_5Te_8$ bulk material (black) and other *A*-type pseudo-hollandite compounds: TlV_5Se_8 (green),[18] $Ba_{0.5}Cr_5Se_8$ (blue),[16] $TlCr_5Se_8$ (red)[15] and $TlIn_5Se_8$ (purple).[60]

Assuming an approximate lattice thermal conductivity of 0.8 $W.m^{-1}.K^{-1}$ for chromium hollandite derivatives of this kind,[16] the expected resistivity for $Cs_xCr_5Te_8$ using the Wiedemann-Franz law and the standard Lorenz factor for metals ($L_0 = 2.44 \cdot 10^{-8}$ $J^2.K^{-2}.C^{-2}$) would be around ρ = 1.2 mΩ.cm at 300 K. This resistivity value is comparable to the reported value of ρ = 0.45 mΩ.cm measured for highly conductive TlV_5Se_8 at the same temperature.[18] It is worth mentioning, however, that Yamazaki and Ueda reported a value of $\rho \sim 1 \cdot 10^2$ mΩ.cm for ACr_5Te_8 (A = K, Rb, Cs) at 300 K.[32] Furthermore, considering that the lattice thermal conductivity is expected to slightly decrease with temperature, the increase observed for the total thermal conductivity suggests a significant rise in the electronic contribution upon increasing temperature. Assuming a rise in resistivity with temperature, which is consistent with a metallic conductive behavior, this observation suggests a dominant temperature-dependent electronic thermal conductivity contribution over that of resistivity, resulting in a gradual increase in resistivity with temperature. However, that eventuality must be confirmed through direct resistivity measurements.

The title compounds show a substantial sensitivity to oxidation and moisture, degrading after a few days under ambient conditions. Therefore, it did not allow us to measure the resistivity and Seebeck coefficient. The latter is expected to be quite low, similar to TlV_5Se_8, given the metallic character of these compounds.

CONCLUSION

The synthesis of single crystals of Cs-filled chromium tellurides revealed the existence of a solid solution within the $Cs_xCr_5Te_8$ composition range (x = 0.73, 0.91 and 0.97). All compositions were found to crystallize in the hollandite-like *B*-type structural form. A detailed crystallographic investigation showed unambiguously that the presence of Cs atoms inside the channels helps in

stabilizing the *B*-type structure. Density functional theory calculations performed on $Cs_{0.75}Cr_5Te_8$ indicated that the non-stoichiometric ACr_5Te_8 compounds (A = Rb, Cs) should be metallic in character with hardly any participation of the alkaline element around the Fermi level. A substantial electronic thermal conductivity can then be expected. As a result, due to an enhanced participation of charge carriers in the thermal transport mechanism, the presence of Cs cations within the channels does not result in a reduction of thermal conductivity compared to that of other *A*-type hollandite derivative compounds.

AUTHOR INFORMATION

Corresponding Authors

Jean-François Halet – orcid.org/0000-0002-2315-4200; Email: jean-francois.halet@univ-rennes1.fr
David Berthebaud – orcid.org/0000-0002-2892-2125; Email: david.berthebaud@cnrs.fr

Authors

Hugo Bouteiller – orcid.org/0009-0004-2132-2962; Email: hugo.bouteiller@univ-poitiers.fr
Bruno Fontaine – Email: bruno.fontaine@ensc-rennes.fr
Takao Mori – orcid.org/0000-0003-2682-1846; Email: mori.takao@nims.go.jp
Franck Gascoin – orcid.org/0000-0002-9791-1358; Email: franck.gascoin@ensicaen.fr

Author Contributions

The manuscript was written through contributions of all authors. All authors have given approval to the final version of the manuscript.

ACKNOWLEDGMENTS

The authors are grateful to the Agence Nationale de la Recherche (ANR – Project HIGHTHERM – Ref ANR-18-CE05-0037) and the Japan Society for the Promotion of Science (JSPS – PE21708) for financial support. Support from JST Mirai Program JPMJMI19A1 is also acknowledged.

Notes

The authors declare no competing financial interest.

REFERENCES

(1) Müller, K. A. Recipe for High-Tc Transition-Metal Chalcogenide Superconductors. *Mater. Chem. Phys.* **1993**, *33* (3–4), 171–175.

(2) Carrig, T. J. Transition-Metal-Doped Chalcogenide Lasers. *J. Electron. Mater.* **2002**, *31* (7), 759–769.

(3) Kagkoura, A.; Skaltsas, T.; Tagmatarchis, N. Transition-Metal Chalcogenide/Graphene Ensembles for Light-Induced Energy Applications. *Chemistry – A European Journal* **2017**, *23* (53), 12967–12979.

(4) Munonde, T. S.; Nomngongo, P. N. Review on Metal Chalcogenides and Metal Chalcogenide-Based Nanocomposites in Photocatalytic Applications. *Chemistry Africa 2023* **2023**, 1–17.

(5) Yadav, S.; Yashas, S. R.; Shivaraju, H. P. Transitional Metal Chalcogenide Nanostructures for Remediation and Energy: A Review. *Environmental Chemistry Letters 2021 19:5* **2021**, *19* (5), 3683–3700.

(6) Guo, Z.; Sun, F.; Yuan, W. Chemical Intercalations in Layered Transition Metal Chalcogenides: Syntheses, Structures, and Related Properties. *Cryst. Growth Des.* **2017**, *17* (4), 2238–2253.

(7) Dai, M.; Wang, R.; Dai, M.; Wang, R. Synthesis and Applications of Nanostructured Hollow Transition Metal Chalcogenides. *Small* **2021**, *17* (29), 2006813.

(8) Hahn, H.; Lorent, C. de. Untersuchungen Über Ternäre Chalkogenide. XII. Über Ternäre Chalkogenide Des Chroms Mit Einwertigem Kupfer Und Silber. *Z. Anorg. Allg. Chem.* **1957**, *290* (1–2), 68–81.

(9) Gautam, U. K.; Seshadri, R.; Vasudevan, S.; Maignan, A. Magnetic and Transport Properties, and Electronic Structure of the Layered Chalcogenide $AgCrSe_2$. *Solid State Commun.* **2002**, *122* (11), 607–612.

(10) Smeggil, J. G. Void Channels in the Nb_3Te_4, Ta_2S, and Nb_2Se Structure Types; the Structure of Nb_3Se_4. *J. Solid State Chem.* **1971**, *3* (2), 248–251.

(11) Hendricks, T.; Caillat, T.; Mori, T. Keynote Review of Latest Advances in Thermoelectric Generation Materials, Devices, and Technologies 2022. *Energies 2022*, **2022**, *15* (19), 7307.

(12) Slack, G. A. in: Semiconductors and Semimetals (Edited by F. Seitz, D. Turnbull and H. Ehrenreich). *Academic Press,* New York, **1979**, *34*, 1.

(13) Mark, J.; Zhang, W.; Maeda, K.; Yamamoto, T.; Kageyama, H.; Mori, T. Ultralow Thermal Conductivity in the Mixed-Anion Solid Solution $Sn_2SbS_{2-x}Se_xI_3$. *J. Mater. Chem. A Mater.* **2023**, *11* (19), 10213–10221.

(14) Hébert, S.; Berthebaud, D.; Daou, R.; Bréard, Y.; Pelloquin, D.; Guilmeau, E.; Gascoin, F.; Lebedev, O.; Maignan, A. Searching for New Thermoelectric Materials: Some Examples among Oxides, Sulfides and Selenides. *J. Phys. Condens. Matter* **2015**, *28* (1), 013001.

(15) Takahashi, H.; Raghavendra, N.; Gascoin, F.; Pelloquin, D.; Hébert, S.; Guilmeau, E. Transport Properties of an Intermetallic with Pseudo-Hollandite Structure as a Potential Thermoelectric Material: The Example of $Tl_xCr_5Se_8$. *Chem. Mater.* **2013**, *25* (9), 1809–1815.

(16) Lefèvre, R.; Berthebaud, D.; Perez, O.; Pelloquin, D.; Hébert, S.; Gascoin, F. Polar Transition-Metal Chalcogenide: Structure and Properties of the New Pseudo-Hollandite $Ba_{0.5}Cr_5Se_8$. *Chem. Mater.* **2015**, *27* (20), 7110–7118.

(17) Lefèvre, R.; Berthebaud, D.; Bux, S.; Hébert, S.; Gascoin, F. Magnetic and Thermoelectric Properties of the Ternary Pseudo-Hollandite $Ba_xCr_5Se_8$ ($0.5 < x < 0.55$) Solid Solution. *Dalton Trans.* **2016**, *45* (30), 12119–12126.

(18) Maier, S.; Lefèvre, R.; Lin, X.; Nunna, R.; Berthebaud, D.; Hèbert, S.; Mar, A.; Gascoin, F. The Solid Solution Series $Tl(V_{1-x}Cr_x)_5Se_8$: Crystal Structure, Magnetic and Thermoelectric Properties. *J. Mater. Chem. C Mater.* **2015**, *3* (40), 10509–10517.

(19) Huster, J. Darstellung Und Kristallstruktur Der Alkalithiochromate (III), ACr_5S_8 (A = Cs, Rb Und K). *Z. Anorg. Allg. Chem.* **1978**, *447* (1), 89–96.

(20) Klepp, K.; Boller, H. Channel Structures Based on Octahedral Frameworks: The Crystal Structure of $TlTi_5Se_8$, TlV_5Se_8, and $TlCr_5Se_8$ and Its Relationships to $TlCr_3S_5$, Hollandites, and Psilomelane. *J. Solid State Chem.* **1983**, *48* (3), 388–395.

(21) Bronsema, K. D.; Jansen, R.; Wiegers, G. A. The Preparation, Crystal Structures and Properties of the Potassium Vanadium Sulfides $K_xV_5S_8$ ($0.5 \leqq x \leqq 0.7$). *Mater. Res. Bull.* **1984**, *19* (5), 555–562.

(22) Bronger, W.; Herudek, C.; Huster, J.; Schmitz, D. New Alkali Metal Chromium Chalcogenides and Their Structural Classification. *Z. Anorg. Allg. Chem.* **1993**, *619* (2), 243–252.

(23) Novet, T.; Wagner, M.; Jiang, M.; Johnson, D. C. The Preparation and Properties of $M'M_5X_8$ (X = Se, Te; M = Cr, Ti; M' = Li, Na, K, Rb, Cs, Cd, Sn, Pb) via Low Temperature Ion Exchange Reaction. *Mater. Res. Bull.* **1995**, *30* (1), 65–73.

(24) Ohtani, T.; Onoue, S. Preparation and Magnetic Properties of the New Ternary Chalcogenides Isotypic with TlV_5S_8 and TlV_6S_8. *Mater. Res. Bull.* **1986**, *21* (1), 69–76.

(25) Ohtani, T.; Sano, Y.; Kodama, K.; Onoue, S.; Nishihara, H. Synthesis of New Ternary Tunnel Chalcogenides by Ion Exchange Reactions and Deintercalation of the Ternary Chromium Selenides. *Mater. Res. Bull.* **1993**, *28* (5), 501–508.

(26) Ohtani, T.; Onoue, S. The Phase Study of the Tl-V-S System and the Properties of TlV_6S_8 and TlV_5S_8 Phases. *J. Solid State Chem.* **1985**, *59* (3), 324–331.

(27) Schramm, W.; Schöllhorn, R.; Eckert, H.; Müller-Warmuth, W. Nonstoichiometric Channel Chalcogenides $Tl_xV_5S_8$: Topotactic Redox Reactions and NMR Studies. *Mater. Res. Bull.* **1983**, *18* (10), 1283–1289.

(28) Quint, R.; Boller, H. On the Crystal Chemistry of Hollandite-like Phases with TlV_5S_8 Structure: The Crystal Structures of $Tl_xTi_5S_8$, $Tl_xV_5S_8$ and $TlCr_5S_8$. *Mater. Res. Bull.* **1987**, *22* (11), 1499–1504.

(29) Fournès, L.; Vlasse, M.; Saux, M. Preparation, Properties and Crystal Structure of TlV_5S_8. *Mater. Res. Bull.* **1977**, *12* (1), 1–5.

(30) Boller, H.; Klepp, K. O.; Kirchmayr, K. On the Knowledge of Two Thallium-Tellurochromites [$TlCrTe_2$ and $TlCr_5Te_8$]. *Mater. Res. Bull.* **1995**, *30* (3), 365–371.

(31) Yamazaki, S.; Ueda, Y. Synthesis, Structures and Magnetic Properties of Pseudo-Hollandite Chromium Sulfides. *J. Solid State Chem.* **2010**, *183* (9), 1905–1911.

(32) Yamazaki, S.; Ueda, Y. New Ferromagnetic Chromium Chalcogenides, ACr_5Te_8 (A = K, Cs and Rb). *Solid State Phenomena* **2011**, *170*, 17–20.

(33) Lefevre, R.; Berthebaud, D.; Gascoin, F. Substitution of Indium for Chromium in $TlIn_{5-x}Cr_xSe_8$: Crystal Structure of $TlIn_{4.811(5)}Cr_{0.189(5)}Se_8$. *Acta Crystallogr. E Crystallogr. Commun.* **2017**, *73*, 500–502.

(34) Gareh, J.; Boucher, F.; Evain, M.; O'Connor, C. J.; Li, S. Synthesis and Crystal Structure of the New Hollandite-like Channel Phase $Rb_{0.73}Cr_5Te_8$. *J. Solid State Chem.* **1996**, *122* (1), 41–45.

(35) Boucher, F.; Gareh, J.; Gourdon, O.; Evain, M.; O'Connor, C. J. Synthesis and Crystal Structure of the Pseudo-Hollandite $Rb_{0.62}Cr_5Te_8$ and Analysis of the Electronic Band Structures of the $Rb_xCr_5Te_8$ Phases. *J. Solid State Chem.* **1997**, *131* (2), 326–334.

(36) Bensch, W.; Sander, B. The Influence of Sulfur and Selenium onto the Physicochemical Properties of the Quasi-Ternary Chromium Chalcogenides $TlCr_5S_{8-z}Se_z$ (z = 0–8). *Solid State Sci.* **2002**, *4* (5), 701–708.

(37) Bensch, W.; Helmer, O.; Näther, C. Evidences for the Formation of Chromium in the Unusual Oxidation State Cr(IV): I. Chemical Reactivity, Microhomogeneity, and Crystal Structures of the Nonstoichiometric Channel Compounds $Tl_xCr_5Se_8$ ($0 \leq x \leq 1$). *J. Solid State Chem.* **1996**, *127* (1), 40–50.

(38) Dung, N.-H.; Tien, V.-V.; Behm, H. J.; Beurskens, P. T. Superstructure with Pseudo Translation. II. Monopotassium Pentachromium Octaselenide: A Tunnel Structure. *Acta Crystallogr. C* **1987**, *43* (12), 2258–2260.

(39) Saßmannshausen, M.; Lutz, H. D. Thermal Motion of the Univalent Metal Ions in KCr_5S_8-Type Chalcogenides, Ternary Chromium Selenides $M_xCr_5Se_8$ (M = Rb, Cs). *Z. Kristallogr.* **2000**, *215*, 683–687.

(40) Gray, D. L.; Ibers, J. A. Synthesis and Structure of $CsTi_5Te_8$: Relation to the TlV_5S_8, $TlCr_3S_5$, and Similar Channel Structures. *J. Alloys Compd.*, **2007**, *440* (1–2), 74–77.

(41) Babo, J.-M.; Schleid, T. Synthesis and Crystal Structure of the Rubidium Scandium Telluride $RbSc_5Te_8$. *Z. Anorg. Allg. Chem.* **2008**, *634* (9), 1463–1465.

(42) Byström, A.; Byström, A. M. The Crystal Structure of Hollandite, the Related Manganese Oxide Minerals, and α-MnO_2. *Acta Crystallogr.* **1950**, *3* (2), 146–154.

(43) Miura, H. The Crystal Structure of Hollandite. *Mineralogical Journal* **1986**, *13* (3), 119–129.

(44) Petricek, S.; Boller, H.; Klepp, K. O. A Study of the Cation Order in Hollandite-like $M_xT_5S_8$ Phases. *Solid State Ion* **1995**, *81* (3–4), 183–188.

(45) Waki, T.; Morimoto, Y.; Kato, H.; Kato, M.; Yoshimura, K. Physical Properties of $Ba_{1.09}V_8O_{16}$ with Hollandite Structure. *Phys. Rev. B Condens. Matter* **2003**, *329–333* (II), 938–939.

(46) Maignan, A.; Lebedev, O. I.; van Tendeloo, G.; Martin, C.; Hébert, S. Metal to Insulator Transition in the n-Type Hollandite Vanadate $Pb_{1.6}V_8O_{16}$. *Phys. Rev. B Condens. Matter Mater. Phys.* **2010**, *82* (3).

(47) Bronsema, K. D.; Mahy, J. One-, Two-, and Three-Dimensional Order in and Four-Dimensional Description of $K_xV_5S_8$ ($0.5 \leqq x \leqq 0.7$). *Phys. Status Solidi (a)* **1987**, *104* (2), 603–618.

(48) Rodriguez-Carvajal, J. Fullprof: A Program for Rietveld Refinement and Pattern Matching Analysis. *Abstract of the Satellite Meeting on Powder Diffraction of the XV Congress of the IUCr* **1990**, 127.

(49) CrysAlis PRO. Oxford Diffraction - Agilent Technologies UK Ltd. Yarnton, England **2014**.

(50) Palatinus, L.; Chapuis, G. SUPERFLIP - A Computer Program for the Solution of Crystal Structures by Charge Flipping in Arbitrary Dimensions. *J. Appl. Crystallogr.* **2007**, *40* (4), 786–790.

(51) Petrícek, V.; Dušek, M.; Palatinus, L. Crystallographic Computing System JANA2006: General Features. *Z. Kristallogr.* **2014**, *229* (5), 345–352.

(52) Kresse, G.; Hafner, J. Ab Initio Molecular Dynamics for Liquid Metals. *Phys. Rev. B* **1993**, *47* (1), 558–561.

(53) Kresse, G.; Furthmüller, J. Efficient Iterative Schemes for Ab Initio Total-Energy Calculations Using a Plane-Wave Basis Set. *Phys. Rev. B* **1996**, *54* (16), 11169–11186.

(54) Kresse, G.; Furthmüller, J. Efficiency of Ab-Initio Total Energy Calculations for Metals and Semiconductors Using a Plane-Wave Basis Set. *Comput. Mater. Sci.* **1996**, *6* (1), 15–50.

(55) Perdew, J. P.; Burke, K.; Ernzerhof, M. Generalized Gradient Approximation Made Simple. *Phys. Rev. Lett.* **1996**, *77* (18), 3865–1868.

(56) Blaha, P.; Schwarz, K.; Tran, F.; Laskowski, R.; Madsen, G. K. H.; Marks, L. D. WIEN2k: An APW+lo Program for Calculating the Properties of Solids. *J. Chem. Physics* **2020**, *152* (7) 074101.

(57) Tran, F.; Blaha, P. Accurate Band Gaps of Semiconductors and Insulators with a Semilocal Exchange-Correlation Potential. *Phys. Rev. Lett.* **2009**, *102* (22), 226401.

(58) Ishtiyak, M.; Jana, S.; Panigrahi, G.; Srivastava, A. K.; Narayanswamy, S.; Bhattacharjee, P. P.; Niranjan, M. K.; Prakash, J. Syntheses, Crystal Structures, Optical, and Theoretical Study of Two Ternary Chalcogenides $CsSc_5Te_8$ and $Cs_{0.6(1)}Ti_6Se_8$ with Tunnel Structures. *Solid State Sci.* **2021**, *114*, 106577.

(59) Fu, B.; Bao, X.; Deng, H.; Zhang, M. Redetermination the Basic Cell Trigonal Cr_5Te_8 Single Crystal Structure and Its Temperature Dependence Raman Spectra. *J. Solid State Chem.* **2021**, *300*, 122222.

(60) Lefèvre, R.; Berthebaud, D.; Pérez, O.; Pelloquin, D.; Boudin, S.; Gascoin, F. Ultra-Low Thermal Conductivity of $Tl_{0.98}In_5Se_8$ and Structure of the New Complex Chalcogenide $Tl_{0.98}In_{13.12}Se_{16.7}Te_{2.3}$. *J. Solid State Chem.* **2017**, *250*, 114–120.